

1 ***EXTRA SPINDLE POLES (Separase) controls anisotropic cell expansion in Norway spruce***
2 ***(Picea abies) embryos independently from its role in anaphase progression***

3

4 Panagiotis N. Moschou¹, Eugene I. Savenkov^{1*}, Elena A. Minina^{1,2*}, Kazutake Fukada^{1*}, Salim
5 Hossain Reza^{1,2}, Emilio Gutierrez-Beltran^{1,2}, Victoria Sanchez-Vera¹, Maria F. Suarez³, Patrick J.
6 Hussey⁴, Andrei P. Smertenko^{5,6} and Peter V. Bozhkov^{1,2}

7

8 ¹Department of Plant Biology, Uppsala BioCenter, Swedish University of Agricultural Sciences
9 and Linnean Center for Plant Biology, PO Box 7080, SE-75007 Uppsala, Sweden ²Department of
10 Chemistry and Biotechnology, Uppsala BioCenter, Swedish University of Agricultural Sciences
11 and Linnean Center for Plant Biology, PO Box 7015, SE-75007 Uppsala, Sweden ³Departamento
12 de Biología Molecular y Bioquímica, Facultad de Ciencias, Universidad de Málaga, 290071
13 Málaga, Spain ⁴The Integrative Cell Biology Laboratory, School of Biological and Biomedical
14 Sciences, University of Durham, Durham DH1 3LE, England, UK ⁵Institute of Biological
15 Chemistry, Washington State University, Pullman, WA 99164, USA ⁶Institute for Global Food
16 Security, Queen's University Belfast, 18-30 Malone Road, 13 Belfast, BT9 5BN, UK

17 *These authors contributed equally to this work

18

19 Corresponding author: Panagiotis N Moschou panagiotis.moschou@slu.se Tel: +46 700780553

20

21 Word count: 5,147, Total; Introduction 627; Material and Methods 1,400; Results 1,988;
22 Discussion 1,132 (21%); Figures 7; Supporting Information: Figures 6, Tables 1, Methods 1, Files
23 1.

24 **Summary**

25 • The caspase-related protease separase (*EXTRA SPINDLE POLES*) plays a major role in
26 chromatid disjunction and cell expansion in *Arabidopsis thaliana*. Whether the expansion
27 phenotypes are linked to defects in cell division in *Arabidopsis ESP* mutants remains elusive.

28 • Here we present the identification, cloning and characterization of the gymnosperm
29 Norway spruce (*Picea abies*) Pa *ESP*. We used *P. abies* somatic embryo system and a combination
30 of reverse genetics and microscopy to explore the roles of Pa *ESP* during embryogenesis in
31 gymnosperms.

32 • Pa *ESP* is expressed in the proliferating embryonal mass, while it is absent in the suspensor
33 cells. Pa *ESP* associates with kinetochore microtubules in metaphase and then with anaphase
34 spindle midzone. During cytokinesis it localizes on the phragmoplast microtubules and on the cell
35 plate. Pa *ESP* deficiency perturbs anisotropic expansion and reduces the size of the stem cell niche
36 in cotyledonary embryos. These functions of Pa *ESP* are independent of its role in chromatid
37 disjunction.

38 • Our data demonstrate that *ESP* functions are evolutionary conserved in gymnosperms and
39 angiosperms, and Pa *ESP* controls embryo development and cell expansion through mechanisms
40 other than segregation of sister chromatids.

41

42 **Keywords:** embryogenesis, cell cycle, microtubules, proteases, separase, spruce

43

44 **Introduction**

45 Embryonic pattern formation in seed plants involves the establishment of apical-basal and radial
46 polarities resulting in the formation of primary shoot and root meristems (Mayer *et al.*, 1991;
47 Meinke, 1991; Ueda and Laux, 2012). Knowledge about plant embryogenesis has benefited from
48 studies of embryo-defective mutants in the angiosperm model species *Arabidopsis thaliana*
49 (Mayer *et al.*, 1991; Capron *et al.*, 2009; Kanei *et al.*, 2012; Wendrich and Weijers, 2013).
50 However, our understanding of the molecular mechanisms underlying embryogenesis remains
51 limited, owing to the restricted accessibility of zygotic embryos during early developmental stages.
52 Somatic embryogenesis represents a valuable model for studying regulation of embryogenesis as
53 it allows synchronized production of a large number of embryos at specific developmental stage
54 and their life imaging (Pennell *et al.*, 1992; von Arnold *et al.*, 2002; Smertenko and Bozhkov,
55 2014).

56 Early embryogenesis in *Arabidopsis* proceeds through highly regular cell division patterns,
57 starting with an asymmetric first division of the zygote, which gives rise to a smaller apical cell
58 and a larger basal cell. The basal cell divides transversely to form a single file of suspensor cells
59 and a hypophysis cell, while the apical cell undergoes several rounds of divisions to give rise to a
60 globular embryo. This stage is followed by the establishment of bilateral symmetry and
61 differentiation of two cotyledons. In most gymnosperms, e.g. Norway spruce (*Picea abies*), the
62 zygote undergoes several rounds of karyokinesis without cytokinesis (free nuclear stage), followed
63 by cellularization and formation of the lowest and the upper cell tiers (Singh, 1978). The lowest
64 tier will form the embryonal mass (gymnosperm equivalent of embryo proper), while the upper
65 tier will form the first layer of suspensor. A fully developed suspensor in spruce embryos is
66 composed of several layers of elongated cells. Unlike *Arabidopsis*, spruce embryos form a crown
67 of multiple cotyledons with radial symmetry surrounding the shoot apical meristem (Singh, 1978).
68 Despite morphological differences in the embryo patterning in different plant lineages, the core
69 regulatory network appears to be conserved (reviewed in Smertenko and Bozhkov, 2014).

70 Previous studies highlighted the importance of proteases in plant embryogenesis and other
71 developmental processes (van der Hoorn, 2008). For example, in *Arabidopsis* a subtilisin-like
72 serine protease ALE1 is required for cuticle formation in the protoderm (Tanaka *et al.*, 2001) and
73 phytocalpain DEK1 is essential for embryogenic cell fate determination (Johnson *et al.*, 2005).
74 *DEK1* mutant embryos that develop beyond globular stage show aberrant cell division planes in

75 the suspensor and embryo proper (Johnson *et al.*, 2005; Lid *et al.*, 2005). In addition, early
76 embryonic patterning in Norway spruce requires the activity of metacaspase mcII-Pa (Suarez *et*
77 *al.*, 2004; Minina *et al.*, 2013). Knockdown of *mcII-Pa* suppresses differentiation of the suspensor
78 and abrogates establishment of apical-basal polarity.

79 Separase (ESP, Extra Spindle Poles) is a caspase-related protease required for
80 embryogenesis in *Arabidopsis* (Liu and Makaroff, 2006) and non-plant species (e.g. Bembenek *et*
81 *al.*, 2010). Initially, ESP was identified as an evolutionary conserved protein that cleaves cohesin
82 to enable disjunction of daughter chromatids during metaphase-to-anaphase transition (referred to
83 as the canonical function of ESP; Ciosk *et al.*, 1998). A temperature sensitive mutant allele of *ESP*
84 from *Arabidopsis* (At *ESP*), *rsw4* (*radially swollen 4*), exhibits a chromosome non-disjunction
85 phenotype (Wu *et al.*, 2010). In addition, *rsw4* causes disorganization of the radial microtubule
86 system in meiocytes (Yang *et al.*, 2011) and defects in anisotropic expansion of root cells
87 associated with radial swelling (Wu *et al.*, 2010).

88 Previously, we examined the role of At ESP in cell polarity and found that At ESP controls
89 microtubule-dependent trafficking that is essential for cell plate synthesis during cytokinesis
90 (Moschou *et al.*, 2013). Here we report the identification and functional characterization of the
91 gymnosperm Norway spruce (*Picea abies*) ESP homologue Pa ESP, and explore the phenotype of
92 spruce embryos depleted of Pa ESP.

93

94 **Materials and Methods**

95 *Plant Material and Growth Conditions*

96 The Norway spruce WT embryogenic cell lines 95.88.22 and 95.61.21, and Pa *ESP*-RNAi lines
97 were cultured as described previously (Filonova *et al.*, 2000). Embryonal masses were separated
98 from the suspensors of seven-day-old embryos using surgical blades in droplets of culture medium
99 under a binocular microscope.

100

101 *Molecular Biology*

102 Primers used in this study are listed in Supplemental Table 1. Full length cDNA of the Pa *ESP* was
103 obtained by 5'- and 3'-RACE with the SMART RACE cDNA Amplification kit (Clontech) and
104 Advantage[®] 2 PCR kit (Clontech) with primers designed from publically available sequences of
105 expression sequence tags (<http://congenie.org/>). Amplified PCR products were cloned into
106 pCR4Blunt-Topo (Invitrogen). The plasmid carrying *FLAG-PaESP* sequence was constructed by
107 ligating 5'-FLAG-PaESP fragment digested with PacI and AatII with 3'-end fragment digested
108 with AatII and Sse8783I into the PacI/Sse8783I-cleaved pAHC25.

109 The *FLAG-PaESP* plasmid was used as template to amplify two overlapping fragments
110 using primers FWPaESPExp1topo-Se-R3 (5'-fragment) and RvPaESPEXPAscI-Se-F2 (3'-
111 fragment). The overlapping region contained a ClaI restriction site. The 5'-fragment was
112 introduced into pTOPO/D vector (Invitrogen) giving rise to the pTOPO/D-PaESP 3.0 kb. The
113 pTOPO/D vector contains an AscI site, upstream of the *attR2* site. The remaining part of Pa *ESP*
114 was introduced by digesting the 3'-fragment by ClaI and AscI and ligating it into pTOPO/D-PaESP
115 3.0 kb digested with ClaI and AscI, thus producing pTOPO/D-PaESP 6.9 kb. The PaESP insert
116 was subcloned into pGWB15 (3xHA-tagged) vector by gateway recombination reaction using LR
117 enzyme.

118 A 2,423-bp long C-terminal fragment was amplified with primers Sep-C-terminus CHis-
119 P, Sep-CHis-M1 and Sep-CHis-M2 from pTOPO/D-PaESP 6.9 kb and introduced into a modified
120 pET11a vector (Quiagen). The pET11a vector was modified by introducing a part from the
121 polylinker of pKOH122 digested with NdeI and BamHI (amplified by pKOH122-MCS-P and
122 MCS-reverse-with-SacI).

123 For constructing Pa *ESP*-RNAi vector, two fragments were amplified using primers
124 FWPaESPExp1topo, PaESPRNAiRV1EcoRI, and FwPaESPRNAiAscI, PaESPRNAiRV2EcoRI.

125 Primer PaESPRNAiRV2EcoRI anneals 400 bp downstream of the PaESPRNAiRV1EcoRI. This
126 400 bp region represents the loop between two arms of the hairpin. The first fragment was cloned
127 in a pTOPO/D vector, which was subsequently digested with EcoRI and AscI and the second
128 fragment was introduced by ligation producing the pTOPO/D-hpRNAiPaESP vector. The hairpin
129 insert was subcloned into a pGWB2 vector (constitutive silencing; Nakagawa *et al.*, 2007) or the
130 pMDC7 [LexA-VP16-ER (XVE) β -estradiol inducible promoter, which is derived from the pER8
131 vector and contains the estrogen receptor-based transactivator XVE; Brand *et al.*, 2006]. The
132 resulting constructs pGWB2-hpRNAiPaESP or pMDC7- hpRNAiPaESP were transformed into
133 *Agrobacterium tumefaciens* GV3101 by electroporation. All constructs were verified by
134 sequencing.

135

136 *Phylogenetic Analysis*

137 Alignments of ESP sequences were performed in ClustalW. Unrooted trees were constructed using
138 the neighbor-joining method (Saitou and Nei, 1987) using the yeast homologue as an out-group.
139 Phylodendrogram was constructed using PAUP software (<http://paup.csit.fsu.edu>). The bootstrap
140 analysis was performed with 2,000 repeats and branches with bootstrap values over 70% were
141 retained.

142

143 *Embryo Transformation and Transient Expression*

144 Norway spruce embryogenic cultures were transformed by *Agrobacterium tumefaciens* GV3101.
145 Agrobacteria were grown overnight in LB medium supplemented with 10 mM MgCl₂, 10 mM 2-
146 (N-morpholino)ethanesulfonic acid (MES) pH 5.5, 40 μ M acetosyringone, 50 μ g mL⁻¹ rifampicin
147 and 50 μ g mL⁻¹ kanamycin. Agrobacteria were collected and incubated for 1 h in 10 mM MgCl₂,
148 10 mM MES pH 5.5, 150 μ M acetosyringone at room temperature on the shaker (OD₆₀₀ = 10). Ten
149 milliliters of five-day-old spruce culture (cell line 95.88.22) were collected in a 50 mL tube and
150 the supernatant was discarded. The spruce culture was co-incubated with 1 mL *Agrobacterium* in
151 10 mL of 10 mM MgCl₂, 10 mM MES pH 5.5, 150 μ M acetosyringone for 8 h without shaking at
152 20°C in darkness. Excess liquid was removed, spruce cells were placed on three layers of sterile
153 filter paper and the upper layer was transferred on half-strength LP medium (Filonova *et al.*, 2008).
154 After 48 h filter paper was transferred onto half-strength LP medium supplemented with 250 μ g
155 mL⁻¹ cefotaxime (Duchefa), and after additional seven days onto the same medium with addition

156 of 15 $\mu\text{g mL}^{-1}$ hygromycin B (Duchefa). Filters were transferred onto fresh medium once a week
157 for consecutive six weeks. Subsequently, cell colonies were transferred onto the medium without
158 filter papers, and grown in the presence of 250 $\mu\text{g mL}^{-1}$ cefotaxime, 400 $\mu\text{g mL}^{-1}$ timentin
159 (Duchefa) and 15 $\mu\text{g mL}^{-1}$ hygromycin B. After colonies were grown to approximately 2 cm in
160 diameter, suspension cultures were established in half-strength LP without selection agents.

161 For transient expression of Pa *ESP*-RNAi, Norway spruce embryogenic cultures were
162 transformed by *Agrobacterium tumefaciens* as described above with minor modifications. The cell
163 line 95.61.21 was used and after cefotaxime treatment for 2 days, cells were fixed and stained with
164 DAPI. As a control, a pMDC32 vector containing the cDNA encoding for monomeric RFP
165 (mRFP) was used.

166

167 *Absolute quantitative RT-PCR analyses*

168 q-RT-PCR was done as previously described (Moschou *et al.*, 2013). For absolute quantification
169 of cDNA molecules in the RT-PCR, *At ESP* or Pa *ESP* in pGWB15 vectors were used as standards.

170

171 *Preparation of Immunogen and Antibody*

172 The pET11a-PaESP construct was transformed in BL21 (*DE3*) RIL (Stratagene) *Escherichia coli*
173 cells. Purification of His-tagged recombinant C-terminal fragment containing C50 domain (1502-
174 2307 aa) of Pa ESP was performed according to manufacturer instructions (Qiagen). Antisera were
175 raised in three mice.

176

177 *Western Blot Analysis*

178 One hundred mg of plant material was mixed with 200 μL of 2x Laemmli sample buffer (Laemmli,
179 1970), kept on ice for 10 min and boiled for 5 min. Samples were centrifuged at 17,000g for 15
180 min. Equal amounts of each supernatant were loaded on 9% or 4-15% gradient polyacrylamide
181 gels and blotted on PVDF (Polyvinylidene fluoride) membrane (see also Supplemental Methods).
182 Anti-Pa ESP and anti-actin C4 were used at dilution 1:1,000 and 1:200, respectively; anti-mouse
183 or anti-rat horseradish peroxidase (HRP)-conjugates (GE Healthcare, Sweden) were used at
184 dilution 1:5,000. Blots were developed using ECL Prime kit (GE Healthcare, Sweden) and imaged
185 in LAS-3000 Luminescent Image Analyzer (Fujifilm, Fuji Photo Film, Germany).

186

187 *Immunocytochemistry and Imaging*

188 Two-day-old early embryos of Norway spruce were fixed in 3.7% (w/v) formaldehyde in
189 microtubule stabilizing buffer (MTSB; 0.1 M piperazine-N,N'-bis(2-ethanesulfonic acid) (PIPES),
190 pH 6.8, 5 mM EGTA, 2 mM MgCl₂) supplemented with 1% (v/v) Triton X-100. Embryos were
191 blocked with phosphate buffered saline Tween-20 (PBST) supplemented with 5% (w/v) bovine
192 serum albumin (BSA; blocking solution). Subsequently, embryos were incubated overnight with
193 anti-Pa ESP, diluted 1:500, and mouse anti-tubulin YL1/2 (AbD Serotec, UK), diluted 1:200 in
194 blocking solution. Specimen were then washed three times for 30 min in PBST and incubated for
195 3 h with goat anti-mouse tetramethylrhodamine isothiocyanate (TRITC) and anti-rabbit fluorescein
196 isothiocyanate (FITC) conjugated secondary antibodies diluted 1:200 in blocking solution. After
197 washing in PBST, specimen were mounted in Vectashield (Vector Laboratories, Burlingame, CA)
198 mounting medium. The samples were examined using a Leica SP5 or Zeiss 710 confocal
199 microscopes. Objective lenses were oil-corrected 63x (NA=1.6) and samples were examined at
200 room temperature.

201

202 *Tissue Sectioning*

203 Cotyledonary embryos were fixed for 2 h at room temperature under vacuum with 4% (w/v)
204 paraformaldehyde in MTSB supplemented with 0.4% (v/v) Triton X-100. The fixative was washed
205 away with PBST buffer, and embryos were dehydrated on ice by 0.85% (w/v) NaCl (30 min) and
206 an EtOH gradient in 0.85% (w/v) NaCl (50, 70, 85, 95 and 100% for 90 min each, 100% overnight
207 and 100% for 2 h). Samples were treated twice with 100% (v/v) xylene at room temperature for 1
208 h each, overnight with 50% (v/v) xylene supplemented with 50% (w/v) histowax at 40-50°C, and
209 100% (w/v) histowax at 60°C, changing twice per day for 3 consecutive days. Samples were stored
210 at 4°C until they were used. 10-µm thick sections were cut using a microtome and placed on poly-
211 lysine coated slides in water droplets. Water was allowed to evaporate overnight at 45°C. Samples
212 were deparaffinised and rehydrated by two washes, 10 min each, in histoclear, two washes, 2 min
213 each, in 100% (v/v) EtOH, followed by EtOH gradient (95, 90, 80, 60 and 30%) in PBS for 2 min
214 each step. Slides were treated for 2 min with H₂O and 20 min with PBS. Sections were blocked
215 and hybridized with antibodies as described above.

216

217 *Microtubule and Image Analysis*

218 Microtubule length was examined by measuring the length of individual end-to-end filaments in
219 Z-stack images. Density of microtubules was calculated by projecting Z-stacks on single planes.
220 The image and pixel analyses were done using ImageJ v1.48 software (rsb.info.nih.gov/ij). Default
221 modules and options were used. Images were prepared using Adobe Photoshop CS6 (Adobe).

222

223 *Statistical Analysis*

224 Graphs were prepared using Excel v2013 (Microsoft) or JMP v11. Statistical analysis was
225 performed with JMP v11. Statistical methods used are indicated in Figure legends.

226

227 **Results**

228 **Identification, cloning and sequence analysis of Pa ESP**

229 All known ESP proteins are encoded by single genes, with the only exception of *Drosophila*
230 *melanogaster* ESP, which contains two subunits encoded by separate genes (reviewed in Moschou
231 and Bozhkov, 2012). The full-length cDNA for Pa *ESP* was isolated by rapid amplification of
232 cDNA ends (RACE), using internal primers that spanned the conserved 3'-end of the gene (File
233 S1). The cDNA was sequenced and found to be 7,248-bp long and contained an open reading
234 frame (ORF) encoding a polypeptide of 2,308 aa with predicted molecular mass of 259 kDa. We
235 deposited Pa *ESP* sequence in GenBank under the accession number HE793991.1. Phylogenetic
236 analysis revealed the monophyletic mode of ESP origin and that Pa ESP belongs to the
237 gymnosperm clade located between mosses and angiosperms (Fig. 1a and File S1). The C-terminus
238 of Pa ESP contains a conserved caspase-related proteolytic domain (Pfam number PF03568; aa
239 1673-2187, $p=7.1e^{-88}$; Fig. 1b) with the His, Cys catalytic dyad typical for all members of CD-clan
240 proteases (Aravind and Koonin, 2002). This proteolytic domain is the most conserved region of
241 Pa ESP exhibiting 30% and 31% identity with the corresponding domains of human and budding
242 yeast homologues, and over 50% identity with plant homologues. The rest of the sequence is less
243 conserved suggesting functional divergence within ESP family. In contrast to mammalian
244 homologues, all plant ESP proteins lack a well-defined Leucine-rich region, which may be
245 responsible for DNA binding (Fig. 1c; Sun *et al.*, 2009). Furthermore, Pa ESP lacks the Ca^{2+}
246 binding EF-hand and 2Fe-2S motives identified in the *Arabidopsis* homologue (Fig. 1c). These
247 differences in the primary sequence combined with monophyletic nature of the phylogenogram
248 suggest that ESP functions were fine-tuned in different lineages during evolution.

249

250 **Pa ESP protein level is developmentally regulated**

251 Early somatic embryos of Norway spruce develop from unorganized multicellular
252 aggregates called proembryogenic masses (PEMs) upon withdrawal of plant growth regulators
253 (PGR), auxin and cytokinin (Fig. 2a). The later stages of somatic embryogenesis resemble those
254 of zygotic pathway and are promoted by abscisic acid (ABA; Filonova *et al.*, 2000). An early
255 spruce embryo is composed of the embryonal mass, tube cells, and the suspensor (Fig. 2a). While
256 the embryonal mass gives rise to the mature embryo, the suspensor is a transient structure
257 undergoing programmed cell death (Filonova *et al.*, 2000). The tube cells are formed by

258 asymmetric division of stem-like cells in the embryonal mass. Each round of cell division produces
259 two daughter cells with distinct fates; one retains proliferative capacity and remains within the
260 embryonal mass, while its sister cell forms a transient type of cells known as tube cells. The tube
261 cells elongate further to form suspensor cells (Bozhkov *et al.*, 2005).

262 To analyze the levels of Pa ESP at successive stages of plant development, we raised an
263 antibody against the C50 catalytic domain of Pa ESP and used it in immunoblotting to detect Pa
264 ESP in samples prepared at distinct stages of embryonic and post-embryonic development. The
265 antibody recognized a protein of ca 260 kDa that corresponds to the predicted size of Pa ESP
266 (Supporting Information, Methods). High levels of Pa ESP were detected in proliferating PEMs in
267 the presence of PGR (+PGR), but not during differentiation of early embryos (-PGR; Fig. 2b), and
268 in the microsurgically separated embryonal masses of early embryos (Fig. 2c). Neither suspensor
269 cells nor distinct parts of seedlings including cotyledons, young needles, hypocotyls and roots
270 contained detectable amount of Pa ESP protein, demonstrating that high levels of Pa ESP are
271 associated with actively proliferating tissues. The level of Pa ESP seems to be regulated at the
272 transcriptional level, since suspensor cells, cotyledons, hypocotyls and roots contained at least five
273 times less Pa *ESP* mRNA levels than the embryonal mass (Fig. S1a).

274

275 **Pa ESP localizes to microtubules and associates with the cell plate during cytokinesis**

276 The intracellular localization of Pa ESP in the meristematic cells of PEMs and early embryos was
277 examined using immunofluorescence microscopy (Fig. 3a). In non-dividing meristematic cells, Pa
278 ESP decorated cortical microtubules (Fig. S2, top images), while during pre-prophase, Pa ESP was
279 found on the pre-prophase band and perinuclear basket of microtubules (Fig. 3a, panel 1). At the
280 beginning of prophase and until the onset of anaphase diffused localization of Pa ESP was detected
281 around mitotic spindle, as well as on the kinetochore microtubules (Fig. 3a, panel 2). At the onset
282 of anaphase, most of Pa ESP was associated with the spindle poles and midzone microtubules (Fig.
283 3a, panel 3 and Fig. 3b). This localization was independent of the fixation method since the same
284 staining pattern was observed after more stringent fixation with methanol/acetone, which exposes
285 epitopes masked by protein folding or interaction with other proteins (Fig. 3b). Densitometry
286 profiling of the anaphase spindle revealed three apparent peaks corresponding to both spindle poles
287 and the midzone (Fig. 3b). During telophase, Pa ESP concentrated in the phragmoplast midzone,
288 where the cell plate is assembled (Fig. 3b, panel 4). A similar localization was observed after the

289 methanol/acetone fixation and the densitometry profiling revealed only one major peak of
290 fluorescence in the phragmoplast midzone (Fig. 3c). Apart from the midzone, Pa ESP colocalized
291 with microtubules at the leading edge of the phragmoplast, whilst missing in the midzone of the
292 leading edge (Fig. 3a, inset in panel 4). At later stages of phragmoplast development, Pa ESP
293 remained at the cell plate after the depolymerization of microtubules (Fig. 3a, panel 5).

294 We examined localization of Pa ESP in the first layer of anisotropically expanding cells
295 adjacent to the embryonal mass, the tube cells. These cells cease proliferation becoming committed
296 to programmed cell death. During the subsequent differentiation steps, the tube cells elongate to
297 form stereotypical suspensor cells (Bozhkov et al. 2005; Smertenko and Bozhkov, 2014; Zhu *et*
298 *al.*, 2014). Pa ESP was absent from these cells (Fig. S2, bottom images), consistent with the finding
299 that Pa *ESP* mRNA level is greatly reduced in the suspensor (Fig. S1a).

300

301 **Pa *ESP* deficiency impairs embryo development**

302 To investigate the role of Pa *ESP* in embryogenesis we produced transgenic lines constitutively
303 expressing a hairpin construct against Pa *ESP* (Pa *ESP*-RNAi; Fig. 4 and Fig. S1b). We could
304 obtain only two viable cell lines (4.1 and 4.2), while the rest of transgenic lines ceased proliferation
305 following initial selection. Both lines exhibited significantly lower levels of Pa ESP (Fig. 4a and
306 Fig. S1b). Knockdown of Pa *ESP* inhibited the development of early embryos from PEMs upon
307 withdrawal of PGR (Fig. 4b). Wild type (WT) cultures contained highly polarized embryos with
308 compact embryonal masses and several files of anisotropically expanding suspensor cells. On the
309 contrary, Pa *ESP*-RNAi lines contained irregularly formed embryonal masses connected to
310 suspensor-like structure composed of cells with impaired anisotropic expansion (Fig. 4c and Fig.
311 S3a). These cells were excluded from the embryonal masses implying that Pa ESP does not affect
312 specification of tube or suspensor cells, but they failed to elongate and formed large suspensor-
313 like structure with significantly more cells in a file, when compared to WT embryos (Fig. S3a).
314 We noticed that some distal cells of the embryo in RNAi lines exhibited apparent signs of cell
315 death (staining with Evan's blue; Fig. S4). However, these cells lacked signs of proper anisotropic
316 expansion.

317 To exclude the possibility that observed phenotype was a consequence of the pleiotropic
318 effects of the constitutive depletion of Pa *ESP*, we generated estradiol inducible Pa *ESP* RNAi
319 lines (Pa *ESP*-XVE>RNAi; Fig. S1a). Depletion of Pa ESP after treatment with estradiol

320 (induction was done from early embryogenesis onwards) induced similar developmental defects
321 as described for constitutive RNAi lines (Fig. S3a, b). Yet, no alteration in embryo morphology
322 was observed in the Pa *ESP-XVE*>RNAi lines in the absence of estradiol. Taken together, these
323 data demonstrate that Pa ESP is essential for anisotropic cell expansion following the first
324 asymmetric cell division during embryogenesis.

325

326 **Pa ESP is required for chromosome disjunction**

327 To investigate the role of Pa ESP in execution of sister chromatid separation, we stained Pa *ESP*-
328 RNAi or Pa *ESP-XVE*>RNAi cells with DAPI (Fig. 5). We failed to identify any discernible
329 chromosomal aberrations suggesting that during selection process we most likely counter-selected
330 for lines that have sufficient levels Pa ESP to sustain cell division. Furthermore, stable
331 transformation with Pa *ESP-XVE*>RNAi also failed suppressing Pa *ESP* below 50% of the original
332 level in 12 lines despite various induction regimes (estradiol concentration ranging from 1 μ M to
333 50 μ M during early embryogenesis).

334 We overcome this limitation by the transient expression of the Pa *ESP*-RNAi construct
335 mediated by *Agrobacterium tumefaciens* (see Material and Methods for the establishment of the
336 protocol). We used a control vector expressing monomeric RFP (mRFP) to estimate the percentage
337 of cells transformed following *A. tumefaciens* transfection. Approximately, 80% showed
338 detectable mRFP expression under confocal microscope. Transient depletion of Pa *ESP* resulted
339 in over 90% reduction of Pa *ESP* levels, when compared to mRFP transfected cells (determined
340 by qRT-PCR; see also Materials and Methods). We assume that some cells should have even
341 higher suppression of Pa *ESP*, considering that ca. 20% of cells may not be transfected with the
342 RNAi construct. Analysis of the transfected cells revealed chromosome non-disjunction phenotype
343 (Fig. 5; 12 of 56 cells examined versus none of 67 in mRFP control) resembling *Arabidopsis rsw4*
344 allele in this context (Moschou *et al.*, 2013). Complementation experiments of *Arabidopsis rsw4*
345 phenotype with Pa *ESP* showed that Pa ESP could rescue chromatid non-disjunction phenotype of
346 *rsw4* (Liu and Makaroff, 2006; Fig. S5d), but failed to rescue the root swelling phenotype (Fig.
347 S5a-c). On the other hand, a point mutant of Pa ESP with a catalytic cysteine-to-glycine mutation
348 failed to rescue chromatid non-disjunction (data not shown). Thus, Pa ESP performs the canonical
349 role of ESP proteins in anaphase progression.

350

351 Pa ESP is essential for the late embryogenesis

352 We next compared the later stages of embryogenesis in WT and Pa ESP-deficient lines (Fig. 6 and
353 Fig. S6). Whereas normally the cotyledonary embryos could be detected following two weeks after
354 transfer to the maturation medium containing ABA, the cotyledonary embryos in Pa *ESP*-RNAi
355 or Pa *ESP*-XVE>RNAi lines formed only after 10 weeks (Fig. 6a and Fig. S6a, b). The
356 cotyledonary embryos that eventually formed in the RNAi lines exhibited a range of morphological
357 abnormalities, including misshaped and missing cotyledons, short hypocotyls, and split embryos
358 (Fig. 6b, c). Histological examination revealed that individual cortical cells in the hypocotyls of
359 the cotyledonary embryos were enlarged, while the meristematic regions were markedly reduced
360 (Fig. 6d, e and Fig. S6c). Microscopic examination of the DNA staining with DAPI revealed the
361 lack of chromosome non-disjunction phenotype in these lines, suggesting that these developmental
362 defects are not caused by chromosomal aberrations. Therefore, the role of ESP in regulating cell
363 expansion seems to be mechanistically unrelated to its role in anaphase progression.

364

365 Pa ESP deficiency affects microtubule stability

366 Since polarized development depends on cell expansion controlled by microtubules, we examined
367 their organization in the elongating suspensor cells. The highly fragmented nature of microtubules
368 in elongating suspensor cells (see also Smertenko *et al.*, 2003) prevented us from drawing
369 conclusions on microtubule architecture in these cells. We analyzed microtubule organization in
370 two cell types of early embryos: (i) the meristematic cells of the embryonal mass and (ii)
371 embryonal tube cells. Knockdown of Pa *ESP* caused no significant alterations in the random
372 organization of cortical microtubules in the embryonal mass cells (Fig. 7a; Smertenko *et al.* 2003).
373 Contrary, cortical microtubules in the tube cells of Pa *ESP*-RNAi showed reduced density and
374 length (Fig. 7a-c). Similarly, the density and length of cortical microtubules in the hypocotyl cells
375 of Pa *ESP*-RNAi cotyledonary embryos were reduced (Fig. 7a-c). Furthermore, while majority (ca
376 70%) of microtubules in the hypocotyl cells of cotyledonary WT embryos were transverse, they
377 became predominantly oblique or longitudinal in the Pa *ESP*-RNAi lines (Fig. 7d, e). Taken
378 together, these results demonstrate that despite significant reduction of Pa ESP expression during
379 cell differentiation, its activity remains critical for the regulation of microtubule organization and
380 for cell elongation.

381

382 **Discussion**

383 **Diversification of ESP proteins**

384 All members of ESP family share caspase-hemoglobinase fold characteristic for CD clan of
385 cysteine proteases, which includes clostripains, legumains, gingipains, caspases, paracaspases and
386 metacaspases (Aravind and Koonin, 2002). Apart of this conserved fold, the primary structure of
387 ESP lacks significant conservation (Fig. S1). For example, Pa ESP is devoid of the Ca^{2+} -binding
388 EF-hand and 2Fe-2S motives found in At ESP. However, whether these motives serve any function
389 remains unclear.

390 Phylogenetic analysis reveals that ESP homologues of green, brown and diatom algae, and
391 land plants form independent clades (Fig. 1a). This pattern suggests that besides the role in
392 daughter chromatid disjunction, ESP evolved specific functions in each lineage. The monophyletic
393 nature of land plant clade indicates that structure and functions of ESP co-evolved with increased
394 complexity of morphology and life cycle. Considering paucity of information on ESP in
395 *Charophytes*, it remains inconclusive whether primary structure of ESP in land plants diverged
396 due to the evolution of phragmoplast, colonization of land, or transition from unicellular to
397 multicellular body plan (Leliaert *et al.*, 2011). The latter reason can however be ruled out because
398 ESP homologues from unicellular green algae form two separate clades and ESP from
399 multicellular brown algae *Ectocarpus siliculosus* does not group together with any other proteins
400 (Fig. 1a).

401

402 **Role of Pa ESP in cell division and microtubule organization**

403 ESP from different lineages reveal variable intracellular localization pattern. Yeast ESP associates
404 with spindle poles and microtubules of anaphase spindle, whereas human ESP was found only on
405 the metaphase spindle poles and then became cytoplasmic in anaphase (Jensen *et al.*, 2001;
406 Chestukhin *et al.*, 2003). *Arabidopsis* ESP associates with microtubules of prophase, metaphase
407 and anaphase spindle, as well as phragmoplast microtubules and cell plate (Moschou *et al.*, 2013).

408 Similar to At ESP, Pa ESP associates with microtubules during interphase, prophase,
409 metaphase and anaphase and then associates with the phragmoplast microtubules, midzone and
410 cell plate during telophase. Interestingly, Pa ESP was missing from the midzone of the
411 phragmoplast leading edge. Therefore, Pa ESP appears to lack binding sites during initiation of
412 the cell plate assembly. Pa ESP remains associated with the cell plate after disassembly of

413 phragmoplast microtubules, suggesting that it might be required for vesicle trafficking to the
414 maturing cell plate. Consistent with this conclusion, At ESP was found to be temporally
415 colocalized with RabA2a-specific endosomes (Moschou *et al.*, 2013).

416 In our experiments constitutive down-regulation of Pa ESP did not result in chromosome
417 non-disjunction and cytokinetic defects observed in other systems, including *Arabidopsis* (Fig. 5;
418 Liu and Makaroff, 2006; Wu *et al.*, 2010; Moschou *et al.*, 2013). Furthermore, despite association
419 of Pa ESP with mitotic microtubule arrays, no discernible abnormalities in their organization were
420 observed in the Pa *ESP*-RNAi lines. The most likely explanation of normal cell divisions in the Pa
421 *ESP*-RNAi lines is the incomplete gene silencing still allowing production of a sufficient amount
422 of protein (Fig. 4a, upper panel) that sustains anaphase transition. Accordingly, more efficient
423 reduction of Pa ESP by using the transient transfection method that we established herein, revealed
424 the requirement of Pa ESP for chromosome disjunction. Therefore, Pa ESP plays a canonical role
425 in anaphase progression. Although in constitutive RNAi lines the level of Pa ESP was sufficient
426 to ensure normal anaphase progression, the reduced number of meristematic cells in the hypocotyls
427 of Pa ESP-deficient embryos suggests that Pa ESP is required for the regulation of meristem size,
428 independently of its role in anaphase.

429 Consistent with the specific functions of ESP in different lineages, Pa ESP failed to rescue
430 the root-swelling phenotype of *Arabidopsis rsw4* although previously this phenotype could be
431 complemented by At ESP (Moschou *et al.*, 2013). Considering that Pa ESP could complement the
432 chromosome non-disjunction phenotype of *rsw4* and its knock down results in the non-disjunction,
433 Pa ESP appears to be a functional homologue of canonical ESP proteins. These findings suggest
434 different molecular mechanisms underlying the functions of ESP in anaphase progression and in
435 controlling anisotropic cell expansion.

436 In contrast to the unaltered microtubule arrays in the embryonal masses, the cortical
437 microtubules in tube cells and especially in epidermis and cortex cells of cotyledonary embryos of
438 Pa *ESP*-RNAi lines exhibited reduced density and length, as well as altered orientation. The
439 hypocotyl cells in the Pa ESP-deficient embryos were bigger than in the WT, indicating that
440 abnormal microtubule organization was associated with irregular cell expansion (Baskin, 2001;
441 Wasteneys, 2004; Baskin and Gu, 2012). This implies that regulation of microtubule dynamics in
442 cells engaged in anisotropic growth are more sensitive to loss of Pa ESP function than proliferating
443 cells of early embryos, which can tolerate the reduced accumulation of Pa ESP. Therefore, Pa ESP

444 could facilitate stabilization of microtubules which define the elongation axis. We assume that Pa
445 ESP function in stabilization of microtubules could be non-cell-autonomous, involving mobile
446 signals produced in meristematic cells. This function of Pa ESP is consistent with our findings that
447 elongating cells with undetectable Pa ESP (e.g. tube cells) are affected when Pa ESP is depleted
448 in proximal meristematic cells (e.g. embryonal mass cells).

449

450 **Pa ESP is required for elongation of the suspensor**

451 Spruce embryo at the early embryogeny stage undergoes polarization and forms two domains with
452 distinct developmental fates: proliferating embryonal mass and terminally-differentiated
453 suspensor, including the uppermost layer of tube cells (Fig. 2a; Bozhkov *et al.*, 2005). Pa ESP
454 protein could be detected using antibody only in the embryonal masses, while the level of protein
455 accumulation in the elongating embryo-suspenders, tube cells, and seedlings was below detection
456 limits. In accordance with the Western blotting data, qRT-PCR demonstrated significant down-
457 regulation of ESP in all organs, but embryonal mass.

458 Our reverse genetics experiments demonstrate that Pa ESP is critically required to sustain
459 cell elongation during embryogeny. Developmental defects induced by Pa ESP deficiency
460 resemble the phenotype of spruce embryos grown in the presence of polar auxin transport inhibitor,
461 1-N-naphtylphthalamic acid (Larsson *et al.*, 2008). For example, in both cases the fate of suspensor
462 cells was affected and supernumerary suspensor-like cells could be detected instead of normally
463 elongating cells. It is tempting to speculate that as in *Arabidopsis* root cells (Moschou *et al.*, 2013),
464 inhibition of Pa ESP perturbs auxin signaling and in this way interferes with cell expansion.

465

466 **Conclusion**

467 Here, we were able to dissect two functions of separase by showing that a gymnosperm homologue
468 could complement chromosome non-disjunction phenotype of *rsw4*, but not the root swelling
469 phenotype. This cell division-unrelated function of separase could be attributed to the regulation
470 of polarized vesicular trafficking. So far no robust molecular markers of cell polarity have been
471 established for gymnosperms, however recent advances in gymnosperm genomics and an
472 increasing number of fully sequenced gymnosperm genomes should help to overcome these
473 limitations (Birol *et al.*, 2013; Nystedt *et al.*, 2013; Zimin *et al.*, 2014).

474

475 **Acknowledgments**

476 Authors are grateful to Tsuyoshi Nakagawa for sharing published research materials and Alison
477 Ritchie for the assistance in preparation of anti-Pa ESP. This work was supported by grants from
478 the VR Swedish Research Council (to P.N.M. and P.V.B.), Pehrssons Fund (to P.V.B.), the
479 Swedish Foundation for Strategic Research (to P.V.B.), Olle Engkvist Foundation (to P.V.B.),
480 Knut and Alice Wallenberg Foundation (to P.V.B.), August T. Larsson Foundation (to A.P.S. and
481 P.V.B.), Hatch Grant WNP00826 (to A.P.S.), and a Spanish Ministry of Science and Innovation
482 grant (AGL2010-15684 to M.F.S). V. S-V was recipient of a FPI fellowship from the Spanish
483 Ministry of Science and Innovation (BES-2008-003592).

484

485 **Author contributions**

486 P.N.M., E.I.S., E.A.M., K.F.M. S.H.R., E.G.-B. and V.S.-V., performed research; P.N.M., A.P.S.,
487 P.V.B., designed research; P.N.M., A.P.S., P.V.B. wrote this article; M.F.S. and P.J.H. offered
488 materials/analytical methods. All authors approved the final version of the manuscript.

489

490 **References**

- 491 **Aravind L, Koonin EV. 2002.** Classification of the caspase-hemoglobinase fold: detection of new
492 families and implications for the origin of the eukaryotic separins. *Proteins* **46**: 355-367.
- 493 **Baskin TI. 2001.** On the alignment of cellulose microfibrils by cortical microtubules: a review
494 and a model. *Protoplasma* **215**: 150-171.
- 495 **Baskin TI, Gu Y. 2012.** Making parallel lines meet: transferring information from microtubules
496 to extracellular matrix. *Cell Adhesion and Migration* **6**: 404-408.
- 497 **Bembenek JN, White JG, Zheng YX. 2010.** A role for separase in the regulation of RAB-11-
498 positive vesicles at the cleavage furrow and midbody. *Current Biology* **20**: 259-264.
- 499 **Birol I, Raymond A, Jackman SD, Pleasance S, Coope R, Taylor GA, Saint Yuen MM,**
500 **Keeling CI, Brand D, Vandervalk BP, et al. 2013.** Assembling the 20 Gb white spruce (*Picea*
501 *glauca*) genome from whole-genome shotgun sequencing data. *Bioinformatics* **29**: 1492-1497.
- 502 **Bozhkov PV, Filonova LH, Suarez MF. 2005.** Programmed cell death in plant embryogenesis.
503 *Current Topics in Developmental Biology* **67**: 135-179.

- 504 **Brand L, Horler M, Nuesch E, Vassalli S, Barrell P, Yang W, Jefferson RA, Grossniklaus U,**
505 **Curtis MD. 2006.** A versatile and reliable two-component system for tissue-specific gene
506 induction in *Arabidopsis*. *Plant Physiology* **141**: 1194–1204.
- 507 **Capron A, Chatfield S, Provart N, Berleth T. 2009.** Embryogenesis: pattern formation from a
508 single cell. *Arabidopsis Book* **7**: e0126.
- 509 **Chestukhin A, Pfeffer C, Milligan S, DeCaprio JA, Pellman D. 2003.** Processing, localization,
510 and requirement of human separase for normal anaphase progression. *Proceedings of the*
511 *National Academy of Sciences of the United States of America* **100**: 4574-4579.
- 512 **Ciosk R, Zachariae W, Michaelis C, Shevchenko A, Mann M, Nasmyth K. 1998.** An
513 ESP1/PDS1 complex regulates loss of sister chromatid cohesion at the metaphase to anaphase
514 transition in yeast. *Cell* **93**: 1067-1076.
- 515 **Filonova LH, Bozhkov PV, Brukhin VB, Daniel G, Zhivotovsky B, von Arnold S. 2000.** Two
516 waves of programmed cell death occur during formation and development of somatic embryos
517 in the gymnosperm, Norway spruce. *Journal of Cell Science* **24**: 4399-4411.
- 518 **Filonova LH, Suarez MF, Bozhkov PV. 2008.** Detection of programmed cell death in plant
519 embryos. *Methods in Molecular Biology* **427**: 173-179.
- 520 **Jensen S, Segal M, Clarke DJ, Reed SI. 2001.** A novel role of the budding yeast separin Esp1 in
521 anaphase spindle elongation: evidence that proper spindle association of Esp1 is regulated by
522 Pds1. *Journal of Cell Biology* **152**: 27-40.
- 523 **Johnson KL, Degnan KA, Walker JR, Ingram GC. 2005.** AtDEK1 is essential for specification
524 of embryonic epidermal cell fate. *Plant Journal* **44**: 114-127.
- 525 **Kanei M, Horiguchi G, Tsukaya H. 2012.** Stable establishment of cotyledon identity during
526 embryogenesis in *Arabidopsis* by ANGUSTIFOLIA3 and HANABA TARANU. *Development*
527 **139**: 2436-2446.
- 528 **Laemmli UK. 1970.** Cleavage of structural proteins during the assembly of the head of
529 bacteriophage T4. *Nature* **227**: 680-685.
- 530 **Larsson E, Sitbon F, Ljung K, von Arnold S. 2008.** Inhibited polar auxin transport results in
531 aberrant embryo development in Norway spruce. *New Phytologist* **177**: 356-366.
- 532 **Leliaert F, Verbruggen H, Zechman FW. 2011.** Into the deep: New discoveries at the base of
533 the green plant phylogeny. *Bioessays* **33**: 683-692.

- 534 **Lid SE, Olsen L, Nestestog R, Aukerman M, Brown RC, Lemmon B, Mucha M, Opsahl-**
535 **Sorteberg HG, Olsen OA. 2005.** Mutation in the *Arabidopsis thaliana* DEK1 calpain gene
536 perturbs endosperm and embryo development while over-expression affects organ development
537 globally. *Planta* **221**: 339-351.
- 538 **Liu Z, Makaroff CA. 2006.** *Arabidopsis* separase *AESP* is essential for embryo development and
539 the release of cohesin during meiosis. *Plant Cell* **18**: 1213-1225.
- 540 **Mayer U, Ruiz RAT, Berleth T, Misera S, Jurgens G. 1991.** Mutations Affecting Body
541 Organization in the *Arabidopsis* Embryo. *Nature* **353**: 402-407.
- 542 **Meinke DW. 1991.** Perspectives on genetic-analysis of plant embryogenesis. *Plant Cell* **3**: 857-
543 866.
- 544 **Minina EA, Filonova LH, Fukada K, Savenkov EI, Gogvadze V, Clapham D, Sanchez-Vera**
545 **V, Suarez MF, Zhivotovsky B, et al. 2013.** Autophagy and metacaspase determine the mode
546 of cell death in plants. *Journal of Cell Biology* **203**: 917-927.
- 547 **Moschou PN, Bozhkov PV. 2012.** Separases: biochemistry and function. *Physiologia Plantarum*
548 **145**: 67-76.
- 549 **Moschou PN, Smertenko AP, Minina EA, Fukada K, Savenkov EI, Robert S, Hussey PJ,**
550 **Bozhkov PV. 2013.** The caspase-related protease separase (*EXTRA SPINDLE POLES*) regulates
551 cell polarity and cytokinesis in *Arabidopsis*. *Plant Cell* **25**: 2171-2186.
- 552 **Nakagawa T, Kurose T, Hino T, Tanaka K, Kawamukai M, Niwa Y, Toyooka K, Matsuoka**
553 **K, Jinbo T, Kimura T. 2007.** Development of series of gateway binary vectors, pGWBs, for
554 realizing efficient construction of fusion genes for plant transformation. *Journal of Biosciences*
555 *and Bioengineering* **104**: 34-41.
- 556 **Nystedt B, Street NR, Wetterbom A, Zuccolo A, Lin YC, Scofield DG, Vezzi F, Delhomme**
557 **N, Giacomello S, Alexeyenko A, et al. 2013.** The Norway spruce genome sequence and conifer
558 genome evolution. *Nature* **497**: 579-584.
- 559 **Pennell RI, Janniche L, Scofield GN, Booij H, Devries SC, Roberts K. 1992.** Identification of
560 a transitional cell state in the developmental pathway to carrot somatic embryogenesis. *Journal*
561 *of Cell Biology* **119**: 1371-1380.
- 562 **Saitou N, Nei M. 1987.** The Neighbor-Joining method-a new method for reconstructing
563 phylogenetic trees. *Molecular Biology and Evolution* **4**: 406-425.

- 564 **Singh HE. 1978.** Embryology of gymnosperms. In: Handbuch der Pflanzenanatomie, Berlin,
565 Germany: Gebruder Borntraeger.
- 566 **Smertenko A, Bozhkov PV. 2014.** Somatic embryogenesis: life and death processes during
567 apical-basal patterning. *Journal of Experimental Botany* **65**: 1343-1360.
- 568 **Smertenko AP, Bozhkov PV, Filonova LH, von Arnold S, Hussey PJ. 2013.** Re-organisation
569 of the cytoskeleton during developmental programmed cell death in *Picea abies* embryos. *Plant*
570 *Journal* **33**: 813-824.
- 571 **Suarez MF, Filonova LH, Smertenko A, Savenkov EI, Clapham DH, von Arnold S,**
572 **Zhivotovsky B, Bozhkov PV. 2004.** Metacaspase-dependent programmed cell death is essential
573 for plant embryogenesis. *Current Biology* **14**: R339-R340
- 574 **Sun YX, Kucej M, Fan HY, Yu H, Sun QY, Zou H. 2009.** Separase is recruited to mitotic
575 chromosomes to dissolve sister chromatid cohesion in a DNA-dependent manner. *Cell* **137**: 123-
576 132.
- 577 **Tanaka H, Onouchi H, Kondo M, Hara-Nishimura I, Nishimura M, Machida C, Machida Y.**
578 **2001.** A subtilisin-like serine protease is required for epidermal surface formation in *Arabidopsis*
579 embryos and juvenile plants. *Development* **128**: 4681-4689.
- 580 **Ueda M, Laux T. 2012.** The origin of the plant body axis. *Current Opinion in Plant Biology* **15**:
581 578-584.
- 582 **van der Hoorn RAL. 2008.** Plant proteases: From phenotypes to molecular mechanisms. *Annual*
583 *Review of Plant Biology* **59**: 191-223.
- 584 **von Arnold S, Sabala I, Bozhkov P, Dyachok J, Filonova L. 2002.** Developmental pathways of
585 somatic embryogenesis. *Plant Cell Tissue and Organ Culture* **69**: 233-249.
- 586 **Wasteneys GO. 2004.** Progress in understanding the role of microtubules in plant cells. *Current*
587 *Opinion in Plant Biology* **7**: 651-660
- 588 **Wendrich JR, Weijers D. 2013.** The *Arabidopsis* embryo as a miniature morphogenesis model.
589 *New Phytologist* **199**: 14-25.
- 590 **Wu S, Scheible WR, Schindelasch D, Van Den Daele H, De Veylder L, Baskin TI. 2010.** A
591 conditional mutation in *Arabidopsis thaliana* separase induces chromosome non-disjunction,
592 aberrant morphogenesis and cyclin B1;1 stability. *Development* **137**: 953-961.

593 **Yang XH, Boateng KA, Yuan L, Wu S, Baskin TI, Makaroff CA. 2011.** The *Radially Swollen*
 594 *4* separate mutation of *Arabidopsis thaliana* blocks chromosome disjunction and disrupts the
 595 radial microtubule system in meiocytes. *Plos One* 6

596 **Zhu T, Moschou PN, Alvarez JM, Sohlberg JJ, von Arnold S. 2014.** Wuschel-related
 597 homeobox 8/9 is important for proper embryo patterning in the gymnosperm Norway spruce.
 598 *Journal of Experimental Botany* **65**: 6543-6552.

599 **Zimin A, Stevens KA, Crepeau M, Holtz-Morris A, Koriabine M, Marcais G, Puiu D,**
 600 **Roberts M, Wegrzyn JL, de Jong PJ, Neale DB, et al. 2014.** Sequencing and assembly of the
 601 22-Gb loblolly pine genome. *Genetics* **196**: 875-890.

602 **Figure legends**

603 **Figure 1. Analysis of Pa ESP sequence.**

604 **(a)** Phylogenetic tree of ESP protein homologues. *Saccharomyces cerevisiae* protein sequence
 605 was used as an out-group. The bootstrap value for all branching points is 100% unless indicated
 606 otherwise. Accession numbers are indicated in Supplemental File 1.

607 **(b)** Alignment of aa sequences corresponding to the C50 proteolytic domain of ESP proteins. At,
 608 *Arabidopsis thaliana*; Rc, *Ricinus communis*; Dm, *Drosophila melanogaster*; Sc, *Saccharomyces*
 609 *cerevisiae*; Ce, *Caenorhabditis elegans*; Sp; *Schizosaccharomyces pombe*; Hs, *Homo sapiens*; Cr,
 610 *Cryptosporidium parvum*; Cm, *Chlamydomonas reinhardtii*; Pa, *Picea abies*. Asterisks denote the
 611 conserved His, Cys dyad.

612 **(c)** Domain organization of selected members of ESP family proteases. C50, proteolytic domain;
 613 LR, Leu-rich domain; EF-hand, helix-loop-helix topology with the ability to bind Ca²⁺; 2Fe-2S,
 614 iron-sulfur cluster.

615

616 **Figure 2. Pa ESP level is developmentally regulated.**

617 **(a)** A schematic model (adapted from Filonova *et al.*, 2000) and corresponding micrographs of
 618 three principal stages of spruce somatic embryogenesis. Red and blue colors denote proliferating
 619 and dying cells, respectively. EM, embryonal mass; PGR, plant growth regulators; ABA, abscisic
 620 acid. Scale bars, 100 µm.

621 **(b)** Western blot analysis of Pa ESP in 2-day-old embryogenic culture grown in the presence
 622 (+PGR) or absence (-PGR) of PGR.

623 (c) Western blot analysis of Pa ESP in the embryonal masses (EM) and suspensors (SUS) of early
624 somatic embryos, as well as in cotyledons (C), young needles (YN), hypocotyls (H) and roots (R)
625 of seedlings. The images of plant material used for protein extraction are shown above the western
626 blot.

627

628 **Figure 3. Intracellular localization of Pa ESP.**

629 (a) Staining of Pa ESP, tubulin, and DNA in the embryonic cells fixed with formaldehyde during
630 prophase (1), metaphase (2), anaphase (3), telophase (4) and late cytokinesis (5). Inset in panel 4
631 shows higher magnification of the phragmoplast leading edge. Arrowhead denotes the absence of
632 Pa ESP in the leading edge. Inset in panel 5 shows maximum projection image with DNA staining.
633 Scale bars, 5 μ m.

634 (b) and (c) Staining of Pa ESP, tubulin and DNA in the embryonic cells fixed with methanol during
635 anaphase (B) and telophase (C). Densitometry scans were performed in the framed areas. Scale
636 bars, 5 μ m.

637

638 **Figure 4. Effect of Pa ESP knockdown on early embryogenesis.**

639 (a) Western blot analysis of Pa ESP in wild type (WT) and Pa *ESP*-RNAi cell lines. The equal
640 loading was confirmed using anti-actin.

641 (b) Ratio of early embryos to PEMs in WT and Pa *ESP*-RNAi lines grown for seven days without
642 PGR. The data show mean \pm standard deviation of triplicate experiments. *, $P < 0.01$; vs WT,
643 Student's *t*-test.

644 (c) Representative dark field microscopy images of early embryos from WT and Pa *ESP*-RNAi
645 lines grown for seven days without PGR. Arrows indicate formation of ectopic files of small cells
646 instead of elongated suspensor cells. EM, embryonal mass. Scale bars, 100 μ m.

647

648 **Figure 5. Chromosomal aberrations in cells with transiently diminished Pa ESP**

649 For detection of chromosomal aberrations cells were fixed and stained with DAPI. Images are
650 from a single representative experiment replicated twice. As a control in transient assays, lines
651 transiently expressing mRFP under a 35S promoter were used. Aberrations were never observed
652 in these transformants. Arrowhead indicates chromosomal aberration. Yellow lines indicate cell
653 wall between chromosomes of daughter cells. trans, transient. Scale bars, 5 μ m.

654

655 Figure 6. Effect of Pa *ESP* knockdown on development of cotyledonary embryos.

656 (a) Time course analysis of cotyledonary embryo formation in WT and Pa *ESP*-RNAi line 4.1.

657 Data are from a single representative experiment, which was repeated twice with similar results.

658 (b) Classes of cotyledonary embryo phenotypes observed in WT and Pa *ESP*-RNAi line 4.1.

659 Normal, cotyledonary embryos showing radial symmetry and average size; weak, cotyledonary

660 embryos with disturbed radial symmetry and decreased size; severe, cotyledonary embryos

661 showing scission and/or loss of radial symmetry and/or size aberrations; mild, in between the weak

662 and severe classes. Scale bars, 5 mm.

663 (c) Frequency distribution of distinct phenotypes of cotyledonary embryos in WT and Pa *ESP*-

664 RNAi line 4.1. Note the absence of normal embryos in the RNAi line. Data are from a single

665 representative experiment, which was repeated twice.

666 (d) Longitudinal sections of hypocotyls of cotyledonary embryos from WT and Pa *ESP*-RNAi line

667 4.1. Shown on the right are enlarged boxed areas. Yellow lines demarcate meristematic regions.

668 Scale bar, 300 μ m.

669 (e) Diameter of hypocotyl cortex cells of cotyledonary embryos from WT and Pa *ESP*-RNAi lines.

670 The data show mean \pm standard deviation of triplicate experiments, each containing at least 10

671 tissue sections. *, $P < 0.01$; vs WT, Student's *t*-test.

672

673 Figure 7. Effect of Pa *ESP* knockdown on the organization of cortical microtubules.

674 (a) Organization of cortical microtubules in embryonal mass and tube cells of early embryos and

675 hypocotyl cells of cotyledonary embryos from WT and Pa *ESP*-RNAi line 4.1. Insets show higher

676 magnification of boxed areas. Scale bars, 10 μ m.

677 (b) and (c) Microtubule length and density (number of microtubules per 10 μ m) in the embryonal

678 tube cells and hypocotyl cells from WT and Pa *ESP*-RNAi line 4.1. The data show mean \pm standard

679 deviation of duplicate experiments, each including 27 (b) or 10 (c) cells analyzed. *, $P < 0.05$; vs

680 WT, two-sided Dunnett's test.

681 (d) Orientation of microtubules (percentage of microtubules in each particular orientation) in the

682 hypocotyl cells from WT and Pa *ESP*-RNAi line 4.1. Data are from a single representative

683 experiment, which was repeated twice, each time including 27 cells analyzed. *, $P < 0.05$; vs WT,

684 Fischer's exact test.

685 (e) Schematic model for the organization of microtubules in the hypocotyls of WT and Pa *ESP*-
686 RNAi embryos. In the WT embryos, microtubules have predominantly transverse orientation and
687 cells expand anisotropically. In the Pa *ESP*-RNAi embryos, microtubules are disorientated, shorter
688 and less dense and cells expand isotropically.

689

690 **Supporting Information**

691 Additional supporting information may be found in the online version of this article.

692 **Fig. S1. Relative expression levels of Pa *ESP* in WT, Pa *ESP*-RNAi or Pa *ESPXVE*> RNAi**
693 **lines.**

694 **Fig. S2. Intracellular localization of Pa *ESP* in interphase embryonal mass cells and**
695 **differentiated tube cells.**

696 **Fig. S3. Width, length and number of tube and suspensor cells and potency for embryo**
697 **formation, as affected by Pa *ESP* deficiency.**

698 **Fig. S4. Evan's blue staining of suspensor cells in WT and Pa *ESP*-RNAi.**

699

700 **Fig. S5. Pa *ESP* does not complement *rsw4* root swelling phenotype but complements the**
701 **chromatid non-disjunction phenotype.**

702

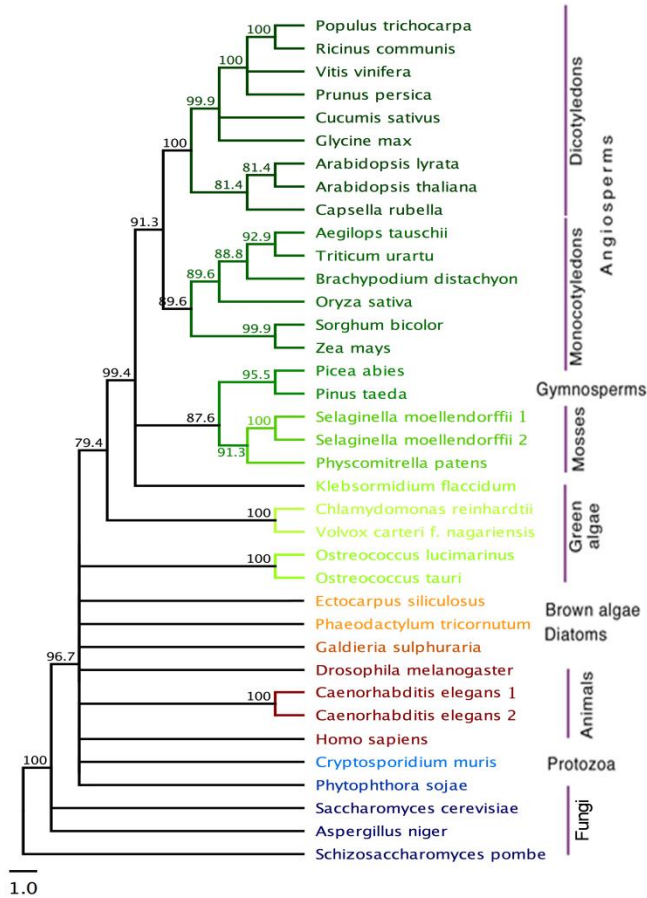
703 **Fig. S6. Effect of inducible Pa *ESP* knockdown on the morphology of cotyledonary embryos.**

704

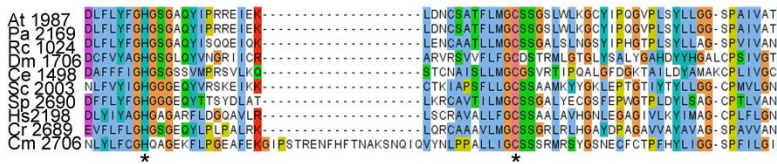
705 **Table S1. List of primers.**

706 **Methods S1. Western blot analysis of Pa *ESP* protein.**

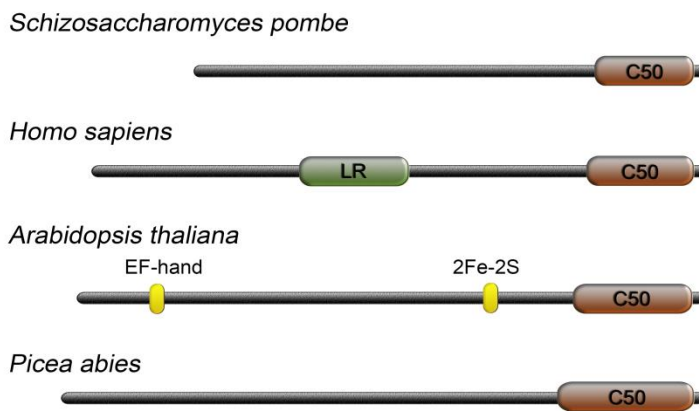
a



b

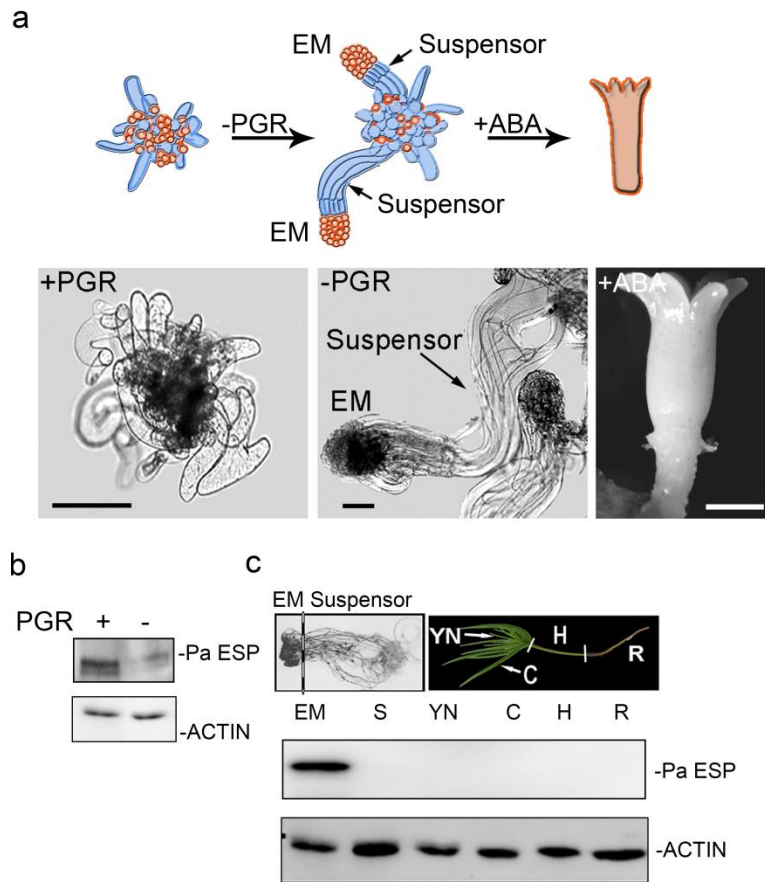


c

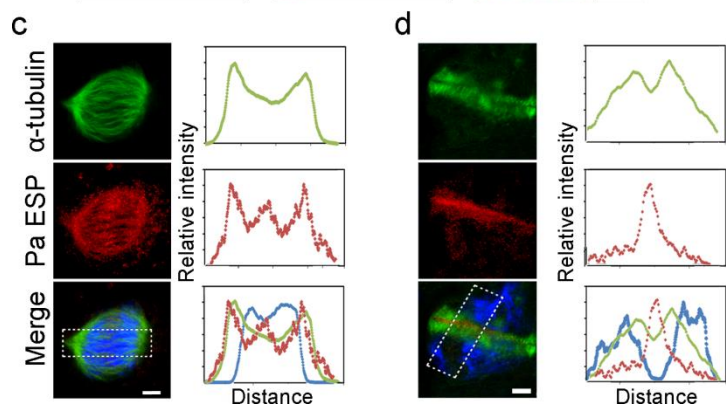
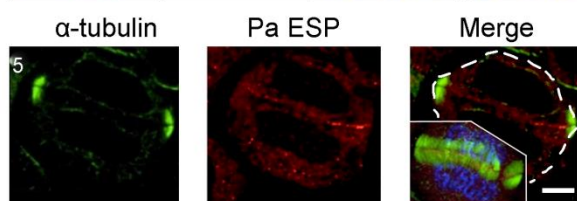
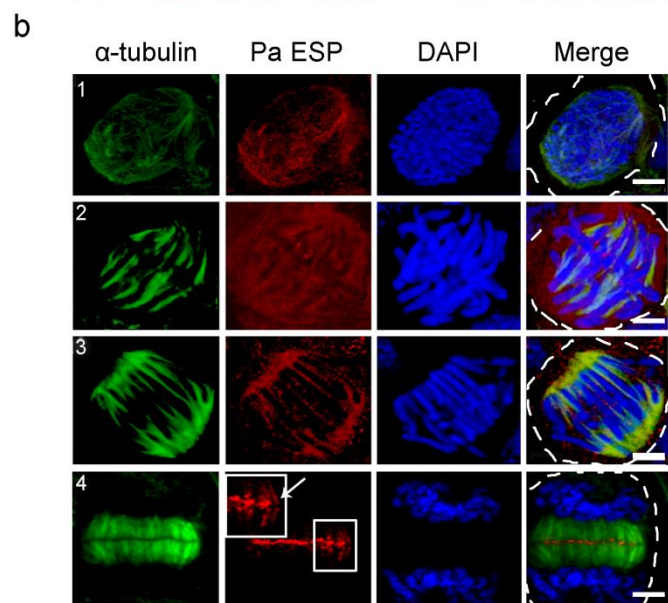
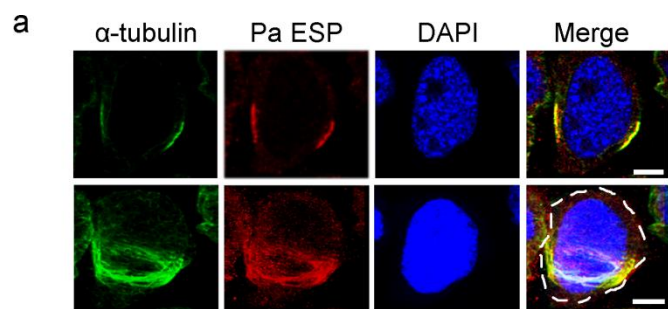


707
708 Fig. 1

250 aa

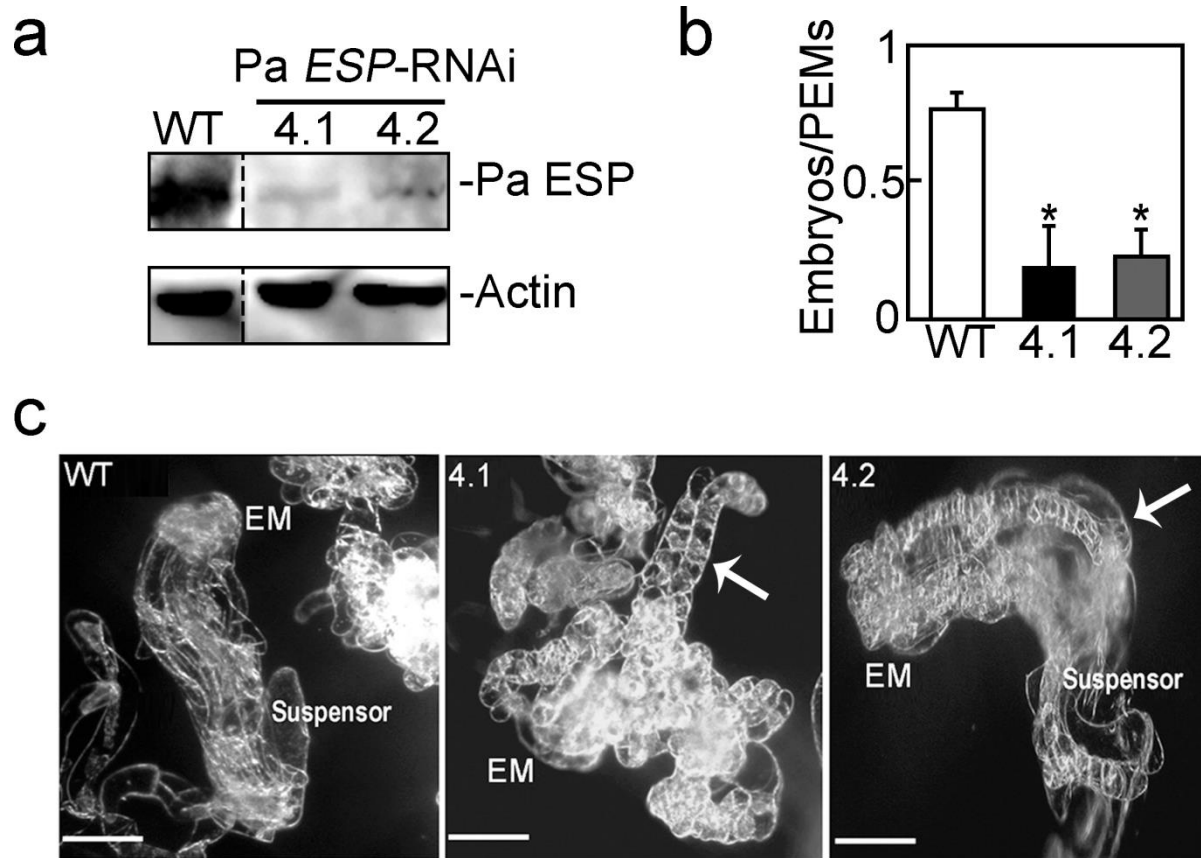


709
710
711



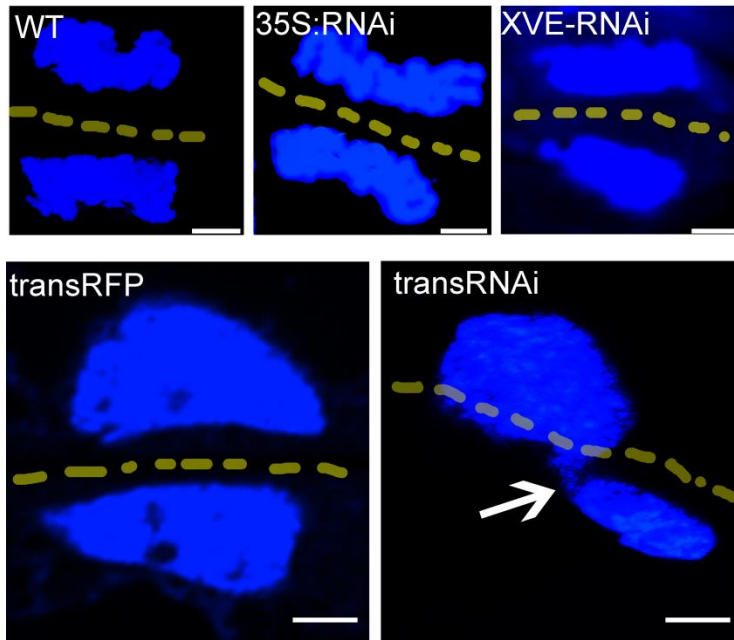
712
713
714

Fig. 3

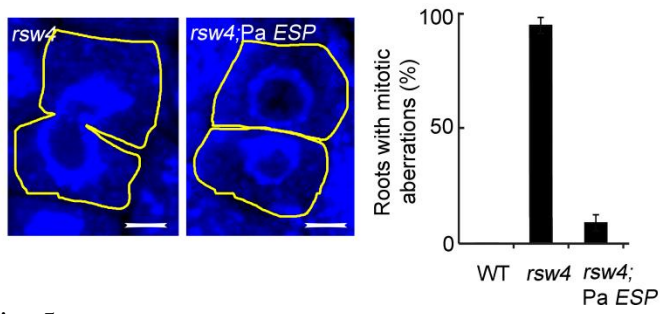


715
716 Fig. 4
717

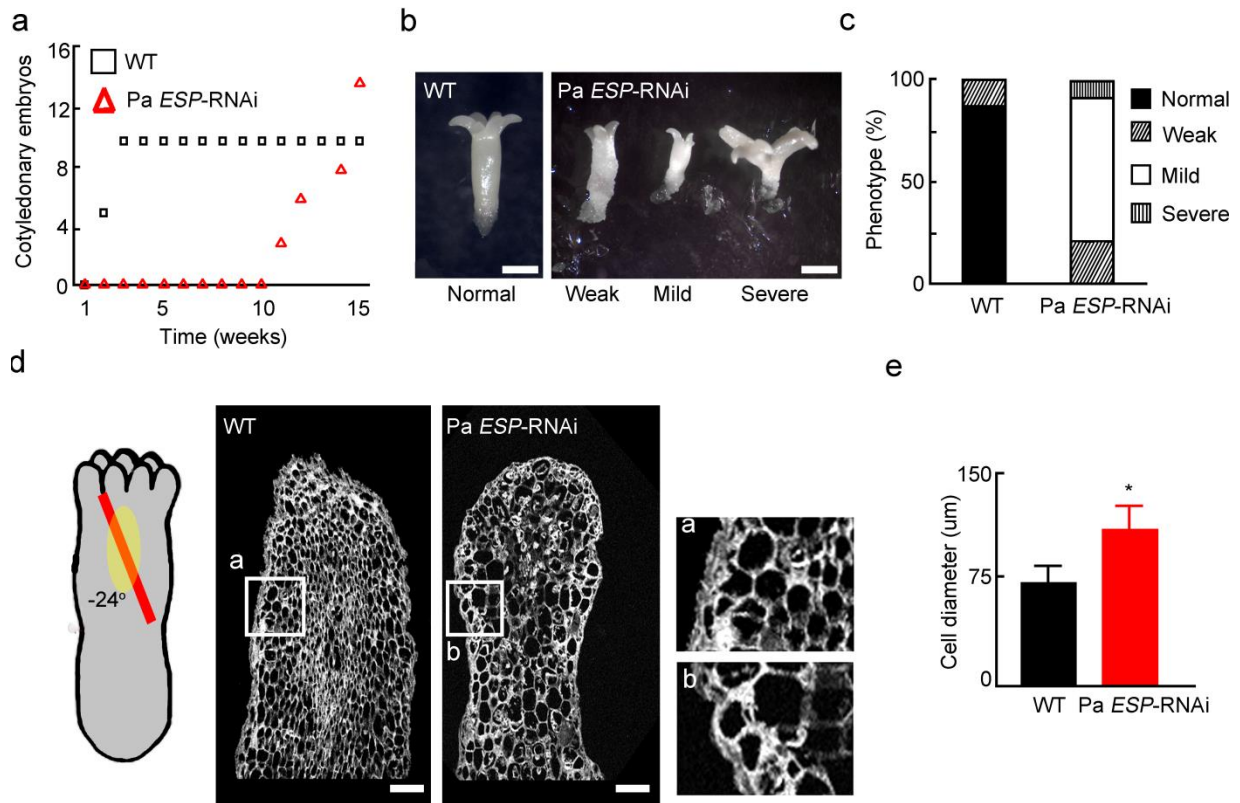
a



b



718
719 Fig. 5
720



721
722 Fig. 6
723

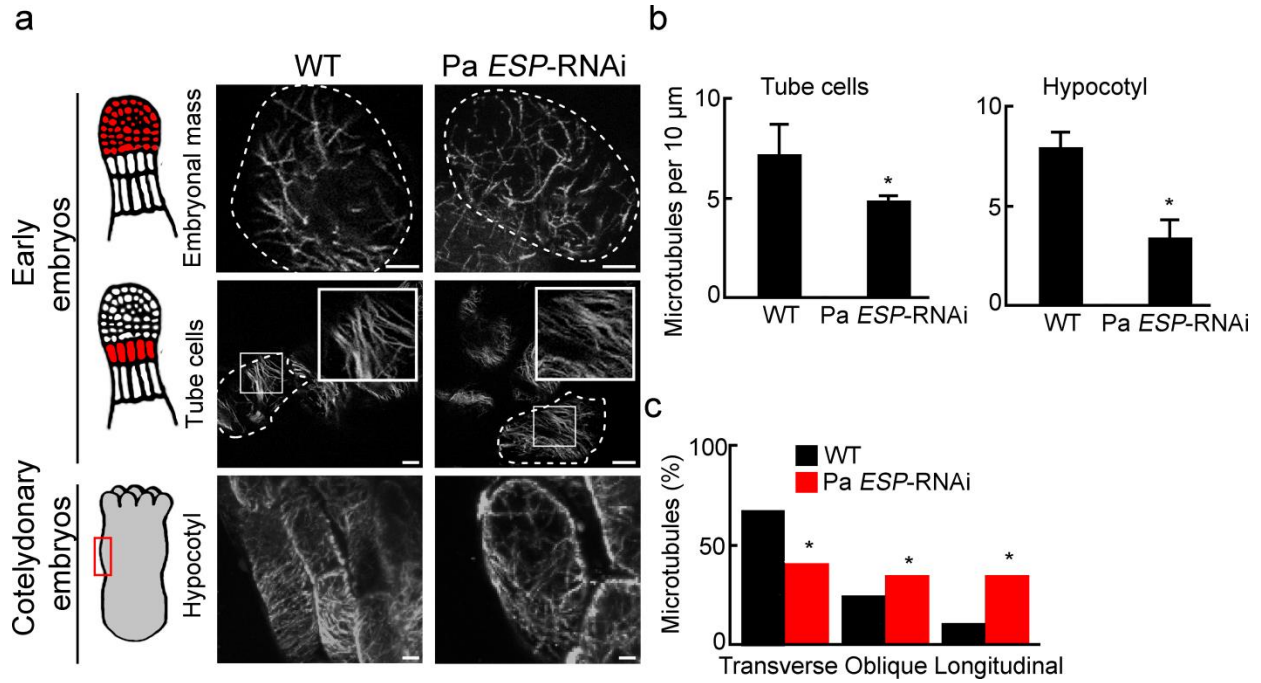


Fig. 7

724
725
726

